PERFORMANCE ASSESSMENT OF ACTIVE AND HYBRID CONTROL BASED ON ENERGY AND SITE POTENTIAL EARTHQUAKES

Xiaozhe Zhang [1], Franklin Y. Cheng [2] and Menglin Lou [3]

[1] *Project Engineer, KPFF Consulting Engineers, Los Angeles, CA, USA*
[2] *Curators' Professor Emeritus of Civil Engg, Missouri University of Science and Technology , Rolla, MO, USA*
[3] *Professor, State Key Laboratory for Disaster Reduction in Civil Engg, Tongji University, Shanghai, China*
Email: szhang@kpff-la.com, fycheng@mst.edu, lml@mail.tongji.edu.cn

ABSTRACT :

The performance evaluation of seismic resistant buildings equipped with structural control is presented in this paper based on probability analysis approach. Due to the uncertainty characteristics of an earthquake, the future ground motion is unlikely to be deterministically predicted at a given site. In the probability analysis, a group of ground motions is produced for each of three earthquake magnitudes of 6, 7, 8. The time history responses are then determined for each input motion in the group and the maximum output are examined using the Monte Carlo method. The distribution of the largest maximum (extreme value) is assumed to follow the Gumbel-type distribution. Here, ground motions are generated considering the earthquake fault and tectonic movements at the building site with the finite-fault stochastic Green's function method. The performance is expressed in terms of the allowable structural displacement under control and the control force requirement as well as the energy demand in the controller. The performance is assessed with the coverage probability by which the control objective is to be evaluated in the concept of probabilities. To perform a lifetime evaluation, the earthquake occurrence model is used to predict the earthquake return period. The method is general for various types of control system, and detailed discussions are illustrated for active and intelligent hybrid controllers. The intelligent strategy is designed for the application of a hybrid control system, composed of the actuator and passive damper. The control operation is triggered with specified threshold response values. Only the passive damper part operates under small and moderate earthquakes so that the active actuator does not need to be activated; the actuator is activated for strong earthquakes when the threshold requirement cannot be satisfied by the passive part alone. Mathematical formulations are presented with numerical results of a six-story building, protected with either active or hybrid control, and subjected to different magnitude of earthquakes. A hundred earthquakes are generated for each of three magnitudes: 6.0, 7.0 and 8.0 on the Richter scale. The intelligent hybrid control reveals its advantage over the active system based on the energy consumption during the building's life-cycle period.

KEYWORDS: Seismic performance, Probability, Control, Energy, Earthquake, Earthquake occurrence

1. PROBABILITY EVALUATION OF BUILDING SEISMIC RESPONSE

For a controlled structure, the maximum peak value of response, such as floor displacement, the control force, etc. under an earthquake is a random variable, X. The probability approach proposed in this paper is a statistical analysis performed by collecting a sample set for X, which is composed of the maxima of all responses caused by each ground motion in the group. The distribution of the largest maximum (extreme value) is based on Gumbel-type distribution, which is the most adopted in engineering practice. It can be used in the dynamic analysis of a civil engineering structure (Penzien and Liu 1969) for which the probability distribution function (PDF) can be expressed as (Kotz and Nadarajah 2000)

$$P_e(\eta_e) = \Pr[X \le \eta_e] = \exp[-\exp(-\alpha(\eta_e - u))] \tag{1.1}$$

The distribution function gives the probability for the variable less than a specific value. The probability density function (pdf) can be found by taking derivation of the variable on PDF. They are described by two parameters, u and α. u is actually the most probable (M.P.) value of the extreme value, η_e, α is another distribution parameter. The PDF in Eqn. 1.1 gives the expression for the coverage probability, P_r, of which X is not larger than η_e. The value, η_e, is solved from Eqn. 1.1 as the expression of the P_r shown below

$$G(P_r) = \eta_e = u - (1/\alpha)\ln(\ln(1/P_r)) \tag{1.2}$$

which is called the percentage point function (PPF) and it gives the expected value of the variable for a coverage probability, P_r. In the statistical analysis, the distribution parameters of u and α can be estimated based on the collected sample set as

$$\tilde{u} = \hat{\bar{\eta}}_e - \sqrt{6}\gamma\hat{\sigma}_{\eta_e}/\pi, \qquad \tilde{\alpha} = \pi/\sqrt{6}\hat{\sigma}_{\eta_e} \tag{1.3a,b}$$

where $\hat{\bar{\eta}}_e$, $\hat{\sigma}_{\eta_e}$, γ=0.5772 are mean value, standard deviation of X, and the Euler-Mascheroni constant, respectively. For the control performance evaluation, the concerned response can be statistically analyzed for both controlled and uncontrolled structural systems and the results can be compared for a given P_r. The distribution for the required control force magnitude can be similarly calculated at that P_r. The method will be demonstrated in the numerical samples.

2. GROUND MOTION GENERATION AT BUILDING SITE

A tectonic earthquake is caused by seismic fault movements. The vibration starts at the rupture in an interface of the fault planes, which causes an earthquake wave and the wave propagates within the earth's crust. When the wave reaches the building site, it appears to be a vibration at the supporting ground of the building. The ground motions can be numerically simulated at a building site per the seismic fault information around the site. The numerical generation of the input ground motion in this study is the finite-fault stochastic Green's function method, based on the information of the seismic fault. The fault plane is supposed to be rectangular as shown in Figure 1 and its location is described by the strike (in degree), dip (in degree), upper edge depth and geographic coordinates at one of its corners. The rupture plane in an earthquake is also supposed to be rectangular located within the fault plane and the finite-source model is applied, in which the rupture plane is discretized into finite elements with dimension of dL×dW and each element treated as a small source. The size of the rupture plane (L×W) and sub-rupture can be determined based on their empirical relations to the earthquake magnitude, earthquake tectonic motion types, such as intraplate,or interplate with and motions of normal, reverse, or strike slip.

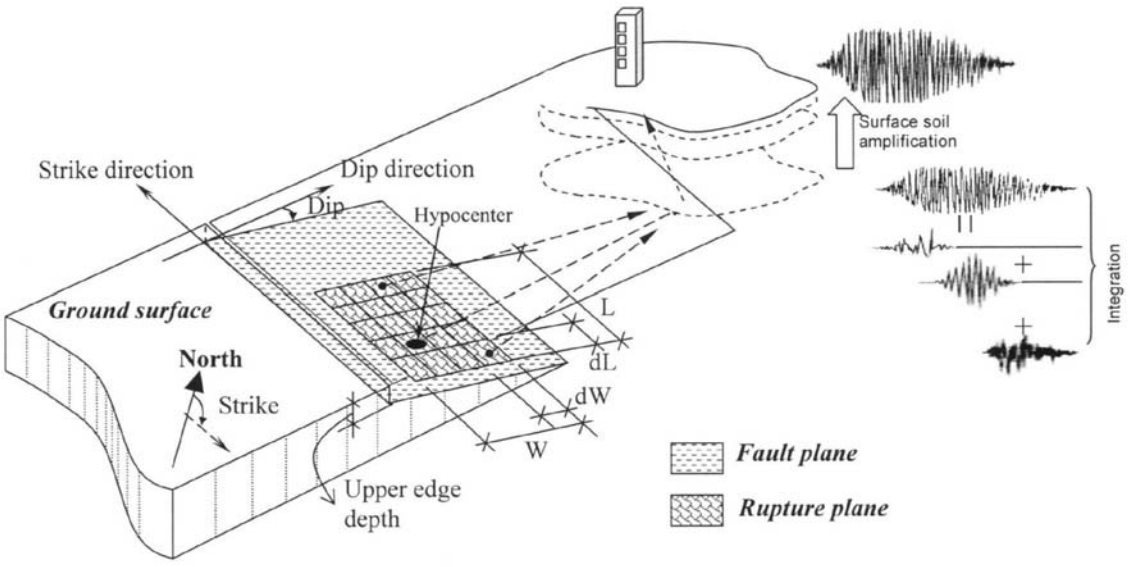

Figure 1 Ground motion generation at the building site

The generation procedure for each ground motion is illustrated in Figure 1. The rupture initiates at the hypocenter (the black dot shown in the figure) at one of the sub-faults and it generates an elastic wave, which propagates to all directions. The rupture at other sub-faults will be triggered when the wave reaches it, and a new wave is generated by itself. Three arrows in the figure are drawn to multiple waves initiated from each sub-fault and propagate to the site. At the bedrock surface under the building site, motions conveyed from all

sub-faults are integrated with proper time delays. Here, the crustal rock is considered as elastic material. The base rock surface motion is finally transformed to site surface motions based on the soil layer profile. In the numerical simulation, the motion from each sub-fault is modeled by the point-source stochastic Green's function which is proposed by Boore 1983. Firstly, a Gaussian white noise is modulated in the time domain. The time history is then transformed into the frequency domain to be multiplied by the acceleration spectrum, $A(\omega)$, and finally transformed back into the time domain. The acceleration spectrum of the shear wave at the distance of R_d from the rupture fault is given as

$$A(\omega) = C_n M_0 S(\omega) P(\omega) \exp(-\frac{\omega R_d}{2Q(\omega)V_s}) / R_d \tag{2.1}$$

where $C_n = (R_{\theta\phi} \cdot FS \cdot RD)/(4\pi\rho V_s^3)$ is a constant with $R_{\theta\varphi}$ of the radiation pattern coefficient; FS=2 of the amplification factor due to the free surface; $RD = 1/\sqrt{2}$ of the reduction factor for partitioning the energy into two horizontal components; ρ and V_s are density and shear velocity, respectively; and $Q(\omega)$ is the propagation factor. M_0 in Eqn. 2.1 is the seismic moment and it is related to the earthquake magnitude, m_j (Purcaru and Berckhemer 1978), and $P(\omega)$ is the high-cut filter used to consider some sharp decreases with increasing frequency at some cutoff frequencies. $S(\omega)$ is source spectrum given as $S(\omega) = \omega^2/(1+(\omega/\omega_c)^2)$ in which ω_c is the corner frequency related to M_0, V_s and strength of high-frequency radiation.

Earthquakes are grouped into several categories specified with m_j, as the center magnitude of a group, e.g. m_j=6.0, 7.0, and 8.0 represent the earthquakes with the moment magnitude within [5.5 6.5], [6.5 7.5], and [7.5 8.5], respectively. The response can then be evaluated for each earthquake magnitude in the expression of probability. The time history responses are determined for each input motion in a group and the maximum output are collected to be a data set. The distribution of the largest maximum (extreme value) is assumed to follow the Gumbel-type distribution and the probability based response can then be calculated by Eqn. 1.2.

3. STRUCTURAL CONTROL AND INTELLIGENT HYBRID CONTROL

The motion equations of an n-story shear building structure with control under horizontal earthquake acceleration input are derived as (Cheng 2001)

$$[M]\{\ddot{x}\} + [C]\{\dot{x}\} + [K]\{x\} = [\delta_a]\{f_a\} + [\delta_p]\{f_p\} + \{\delta_r\}\ddot{x}_g \tag{3.1}$$

where $\{x\}$ is the vector of floor displacement; [M], [C], and [K] are mass, damping and stiffness matrices, respectively; $\{f_a\}$, $\{f_p\}$, and $\ddot{x}_g$ are active, passive input force vectors, and ground motion acceleration, respectively; $[\delta_a]$, $[\delta_p]$, and $[\delta_r] = -[M]\{I_n\}$ are the input location matrices for active, passive forces and ground acceleration inputs, respectively; and $\{I_n\}$ is a unit vector in order of n. For the active controlled case, the optimal control can be obtained with the generalized optimum control algorithm (GOAC) (Cheng *et al.* 2008) and the linear quadratic regulator (LQR). As for the hybrid control system, the viscoelastic damper is applied as the passive part, while the active control force is determined based on the LQR technique. The dynamic properties of a damper can be mathematically modeled by Maxwell model (Darby 1976, Cheng *et al.* 1996, Soong and Dargush 1997) as

$$\lambda_0 \dot{f}_p(t) + f_p(t) = C_0 \dot{\Delta}_p(t) \tag{3.2}$$

where $f_p(t)$ and $\Delta_p(t)$ are the passive force on the damper and the piston displacement, respectively; C_0 is the passive damping coefficient; and λ_0 is the relaxation time.

The application of the hybrid control is regulated by an intelligent strategy (Zhang *et al.* 2004, 2006), which is designed to maximally use the passive damper and the active energy is saved with specified threshold response values. Only the passive damper part operates under small and moderate earthquakes so that the active actuator does not need to be activated; the actuator is activated for strong earthquakes when the threshold requirement cannot be satisfied by the passive part. The whole control process is divided into three possible stages, and the system automatically switches from the lower stages to the next when responses exceed some prescribed

threshold values. The threshold value can be set for a concerned response such as floor displacement, acceleration, or story drift. There are two threshold values needed to define the three stages.

The working procedure is described as: 1) set two thresholds for the selected response; 2) the system stays in stage 1 for small and some moderate earthquakes, in which only the passive part works and keeps the response lower than the first threshold; 3) the actuator starts to work whenever the response exceeds the first threshold values and the system goes into stage 2; 4) the system moves from stage 2 to stage 3 to generate higher level active force when the response exceeds the second threshold value.

4. ENERGY FORMULATION AND CONTROLLER EVALUATION

To obtain the energy representation of the system, the individual force item in the motion equation, Eqn. 3.1, is integrated over its corresponding displacement as

$$\int \{dx\}^T [M]\{\ddot{x}\} + \int \{dx\}^T [C]\{\dot{x}\} + \int \{dx\}^T [K]\{x\} = \int \{dx\}^T [\delta_a]\{f_a\} + \int \{dx\}^T [\delta_p]\{f_p\} + \int \{dx\}^T \{\delta_r\}\ddot{x}_g \qquad (4.1)$$

in which the first item is the kinetic energy as $\int \{dx\}^T [M]\{\ddot{x}\} = E_k = \frac{1}{2}\{\dot{x}\}^T [M]\{\dot{x}\}$; the second item is the dissipative energy caused by the inherent damping as $\int \{dx\}^T [C]\{\dot{x}\} = E_d = \int \{\dot{x}\}^T [C]\{\dot{x}\}dt$; the third item is the elastic strain energy as $\int \{dx\}^T [K]\{x\} = E_s = \int \{x\}^T [K]\{\dot{x}\}dt$. At the right-hand side, the first item is the energy caused from the active force and represents the input energy from the active control system as $\int \{dx\}^T [\delta_a]\{f_a\} = E_{fa} = \int \{\dot{x}\}^T [\delta_a]\{f_a\}dt$; the second item at the right-hand side is the dissipative energy by the passive damper as $\int \{dx\}^T [\delta_p]\{f_p\} = E_{fp} = \int \{\dot{x}\}^T [\delta_p]\{f_p\}dt$ and the last item is the earthquake input energy as $-\int \{dx\}^T [M]\{I_n\}\ddot{x}_g = E_i = -\int \{\dot{x}\}^T [M]\{I_n\}\ddot{x}_g dt$. The energy balance representation of the controlled system in Eqn. 4.1 is then written as

$$E_k + E_d + E_s = E_{fa} + E_{fp} + E_i \qquad (4.2)$$

The capacity requirement of the active controller for both active and hybrid systems is evaluated in this paper based on energy consumption, expressed as E_{fa}/cyl, which is the total active consumption of energy in the whole earthquake duration divided by the number of cycles of the motion duration. The cycle is used here as the weighting factor, because the response motion cycle varies for individual ground excitations. Thus, the expected energy value per cycle for each group of earthquakes is used for comparison measurement, and also the maximum control force at a given probability obtained for that group.

The expected energy consumption of controllers and the corresponding earthquake input energy, during the whole life of a building are evaluated and compared herein for hybrid and active control systems. This can be viewed as a factor of how much the building is relied on the active system in its life. The accumulated energy is the summation of the energies from each magnitude earthquake, and only earthquakes with magnitude m_j=6.0, 7.0 and 8.0 are considered.

The annual occurrence rate of earthquakes for magnitude m_j is considered by an integer number of events occurring within a year, which is denoted as r(m_j). The Poisson model is proper for earthquake with magnitude m_j=6.0 and 7.0. For infrequent earthquakes such as magnitude m_j=8.0, the non-Poisson renewal model is more appropriate (Anagnos and Kiremidjian1988). Among the non-Poisson renewal models, the Brownian passage time model is often used (Ellsworth and Matthews 1999).

5. NUMERICAL SAMPLES

5.1. Building Properties, Fault and Ground Motion Generation

A six-story shear building is employed for numerical study, which has mass of 1.1×10^5kg for each floor, the

column stiffness of 3.51×10^8, 2.25×10^8, 1.70×10^8, 1.24×10^8, 0.88×10^8, and 0.60×10^8 N/m, for the first through sixth stories, the story height of 3.75m for each floor, and 2% damping ratio. The building site is at geographic coordinates of 139.67ºE, 35.69ºN, where the seismic fault is the Sagami trough between the Philippine Sea plate and the Eurasia plate. More than 100 earthquakes equal or larger than magnitude m_j=6.0 were recorded on the fault in last 400 years (Takahashi *et al.* 2002, Zhang *et al.*2004). The fault plane is rectangular with size of 222km×167km, of which the dip and strike are 15º and 290º, respectively. The upper edge depth is 2.6km below ground level. The geographic coordinates of the south-east corner is 140.50ºE, 34.5ºN. The interplate earthquake is considered and the rupture plane size is decided based on Sato 1979, as $L=10^{0.5mj-1.88}$ and $W=L/2$. dL and dW can be assumed to be same, with d$L=10^{0.4mj-2}$ (Beresnev and Atkinson 1999).

One hundred ground motions are generated for each earthquake magnitude of m_j=6.0, 7.0 and 8.0, respectively. So there are three groups of ground motions, each sample set has a size of 100. The maximum, minimum, mean and standard deviations of the peak ground motion (PGA) for each magnitude earthquake are given in Table 5.1.

Table 5.1 PGA (m/s^2) of ground motions

m_j	Mean	Max	Min	σ_{PGA}
6.0	0.057	0.138	0.019	0.026
7.0	0.156	0.332	0.050	0.066
8.0	0.296	0.425	0.170	0.058

5.2. Control Performance Evaluation

5.2.1 Active control

There are two active controllers placed on the top two floors based on optimal placement evaluation (Cheng *et al.* 2008). Two active cases are studied causing the top floor displacement response reduction of about 20% and 40%, and are called cases of low active and high active, respectively. The time history analyses are performed for each of the individual 100 ground motions in the three groups, from which the maximum responses are collected in each group as the sample sets. The distribution curves are obtained in terms of response and probabilities.

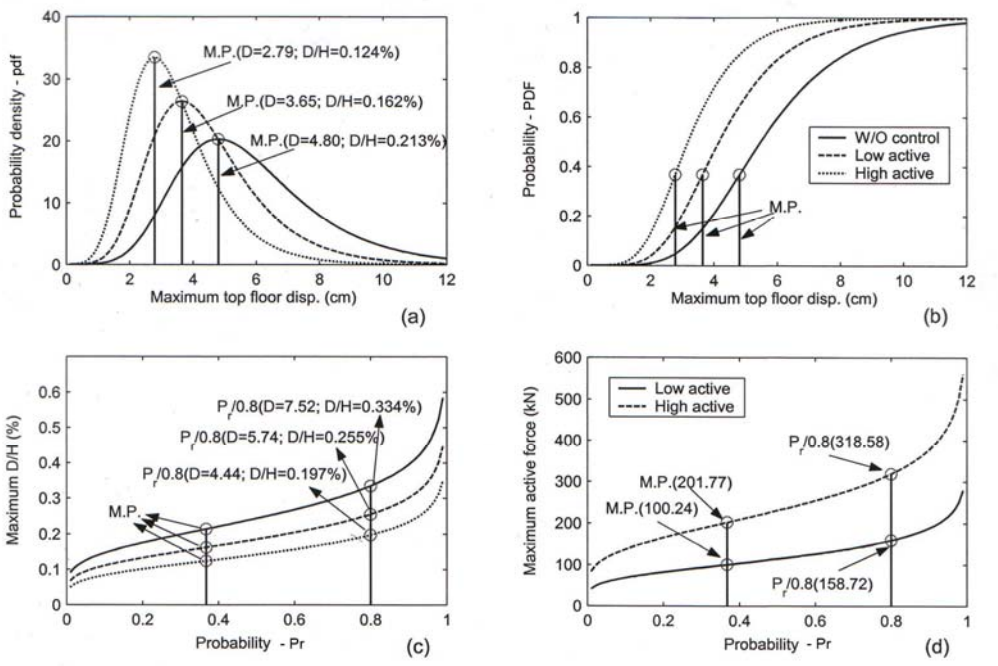

Figure 2 Probability results for active control cases under m_j=7.0 earthquake

For two cases of low active and high active controls, the studies are conducted on the responses of top floor

displacement (denoted as D) and the control force. Similar response phenomena are observed for the other control force, and are not shown here. Due to space limits, only the results under the group with magnitude m_j=7.0 are illustrated and discussed, with the distribution curves drawn in Figure 2. pdf, PDF, and PPF curves of D are given in Figure 2 (a), (b) and (c), respectively, and PPF of the control force is given in the accompanying Figure 2 (d). There, D/H is the ratio of top floor displacement to the building height, H. In the pdf curves, the peaks appear at the most probable (M.P.) values, u, and M.P. is actually the response for the coverage probability of P_r=0.375, as shown in the PDF and PPF curves.

PPF curves present the response values, with respect to the corresponding coverage probability, P_r. The maximum response increases when P_r increases, but the slope becomes large when P_r is close to one. In this paper, the evaluation is based on the response value at P_r=0.8, which means there is a probability of 20% that the response is larger than the value and it is denoted as P_r/0.8. As shown in Figure 2 for m_j=7.0 earthquake, the P_r/0.8 values of D are reduced from 7.52cm of the without control case to 5.74cm (76.3% of the uncontrolled value), and 4.44cm (59.0% of the uncontrolled value) in low active and high actives, respectively. The P_r/0.8 values of the control forces are 158.72kN and 318.58kN in low active and high active.

5.2.2 Hybrid control

In the hybrid control system, two identical controllers, located at the top two floors, have the passive damper with coefficients of C_0=3.84×10^{6}N-s/m and λ_0=0.063s expressed in Eqn. 3.2. In application of the intelligent algorithm, the threshold quantities are assigned for D/H as 0.2% and 0.3% (D=4.5cm and 6.75cm), corresponding to the 1st and 2nd thresholds, respectively.

While performing the time history response for each input motion in a group, the activation of the active system depends on the structural response in comparison to the threshold value that is regulated by the intelligent algorithm. For example, 69 earthquakes in 100 excited only the passive system as stage 1; 27 caused the system to be activated at stage 2; and 4 earthquakes excited the system to be at stage 3, for the input earthquake with magnitude of m_j =7.0. Figure 3 shows the PPF curves of D/H and control forces. Corresponding to P_r/0.8, D/H are 0.214% and 0.334% for control and without control cases, respectively. The active forces in stage 2 and stage 3 are, 168.39 kN and 709.92 kN, respectively and passive force is 205.35 kN at both stages.

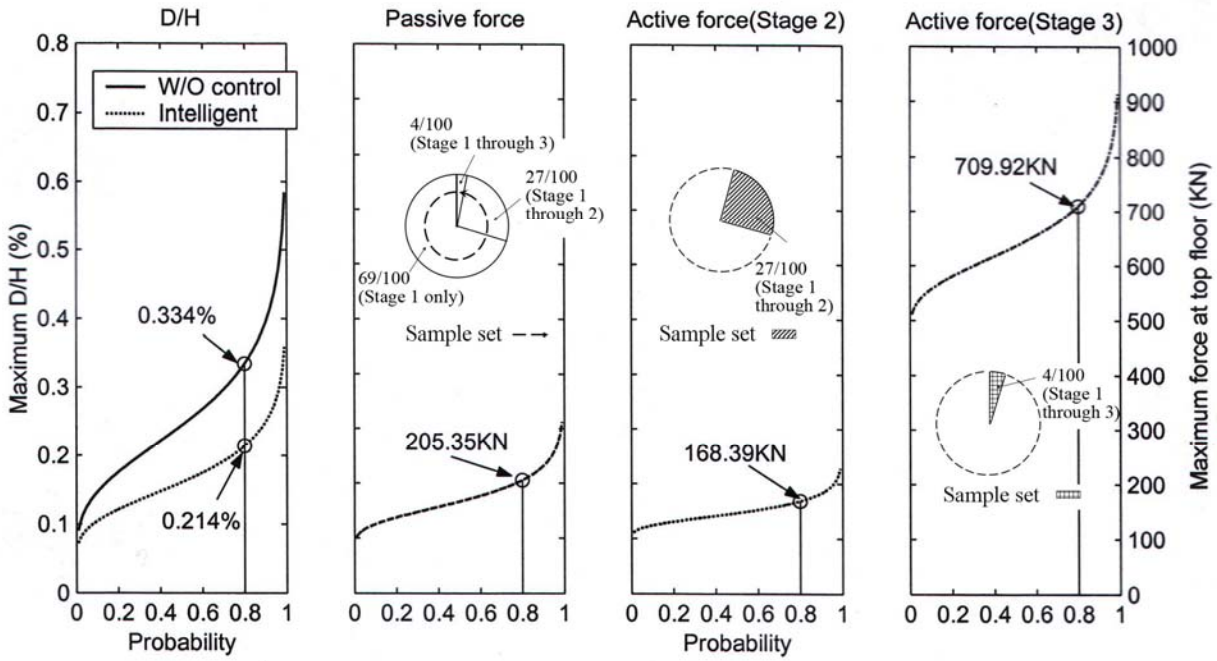

Figure 3 Probability results for hybrid control cases under m_j=7.0 earthquake

5.3. Capacity Assessment of Active Controller in Active and Hybrid Systems

The active energies are calculated for the three groups of earthquakes m_j=6.0, 7.0 and 8.0. In order to compare

active controller capacity requirement, the structural top floor displacement, D, would set to be the same for both control systems. The procedure is to get the same value of D at P_r/0.8 for the two different systems to find the required E_{fa}/cyl and active control forces. In this example, the active control system is still based on low and high control conditions presented in sect 5.2.1.

In comparison conducted with the low active control case, the mean value, σ (standard deviation), and the value at P_r/0.8 for D are shown in Table 5.2. It is found that the passive damper acting alone in the hybrid control system makes the response of D smaller than that obtained by the low active control. Taking m_j=7.0 earthquake as example, the mean value of D equals to 3.99cm in hybrid control case with the passive damper working alone, which is smaller than the value of 4.45cm responded in low active control case. The smaller values are also obtained for σ and the value at P_r/0.8; they are 1.62cm versus 1.78cm and 5.16cm versus 5.74cm. Therefore, no active controller is required in the hybrid system to reach the same reduction realized by the low active control case. E_{fa}/cyl and force magnitude in the hybrid control comparing to the low active control are listed in Table 5.4, in which zero active response is exhibited in the hybrid system.

Table 5.2. Controlled response D in hybrid and low active controls

Earthquake	m_j=6.0		m_j=7.0		m_j=8.0	
Control / Response	Active	Hybrid	Active	Hybrid	Active	Hybrid
Mean (cm)	1.37	1.26	4.45	3.99	8.39	8.02
σ (cm)	0.62	0.56	1.78	1.62	2.75	2.67
Pr/0.8 (cm)	1.81	1.66	5.74	5.16	10.37	9.95

Table 5.3 Controlled response D in hybrid and high active controls

Earthquake	m_j=6.0		m_j=7.0		m_j=8.0	
Control / Response	Active	Hybrid	Active	Hybrid	Active	Hybrid
Mean (cm)	1.02	1.02	3.32	3.40	6.82	6.78
σ (cm)	0.44	0.44	1.41	1.38	2.07	2.11
Pr/0.8 (cm)	1.34	1.34	4.44	4.42	8.31	8.30

Table 5.4. Comparison of actuator capacity in hybrid and low active controls

Earthquake	m_j=6.0		m_j=7.0		m_j=8.0	
Capacity / Control	Force (kN)	E_{fa}/cyl (N-m)	Force (kN)	E_{fa}/cyl (N-m)	Force (kN)	E_{fa}/cyl (N-m)
Active control	52.24	71.62	158.72	734.04	278.25	3729.6
Hybrid control	0	0	0	0	0	0

Table 5.5 Comparison of actuator capacity in hybrid and high active controls

Earthquake	m_j=6.0		m_j=7.0		m_j=8.0	
Capacity / Control	Force (kN)	E_{fa}/cyl (N-m)	Force (kN)	E_{fa}/cyl (N-m)	Force (kN)	E_{fa}/cyl (N-m)
Active control	100.97	78.06	318.58	926.32	577.91	5537.7
Hybrid control	57.11	34.10	149.55	338.44	380.15	2870.7

In comparison conducted with the high active control case, the same controlled responses are obtained for D (P_r/0.8) as shown in Table 5.3, for which E_{fa}/cyl and force magnitude for both systems are calculated and given in Table 5.5. The results reveal that the active controller requires much less capacity in the hybrid system than in the active system. Taking the results of m_j=7.0 earthquake as an example, the required active force is 318.58 kN for the active system, which is 2.13 times the required force, at 149.55kN, in the hybrid system. The energy, E_{fa}/cyl=926.32 N-m, in the active system is 2.73 times of that in the hybrid system, 338.44kN.

Apparently, the active controller capacity requirement can be reduced in the hybrid control system. The saving of the active controller's capacity depends on the passive damper capacity and the amount of expected response

reduction.

5.4. Accumulative energies in Building Life Time

Based on the investigation of the history data of the earthquakes occurring within a fault plane, the annual occurrence rates for the three earthquake magnitudes are obtained. The expected energy can be calculated per Eqn. 4.1. The expected input energy for an earthquake in magnitude m_j is the average of that induced by each motion in the group. In Figure 4, group A shows the lifetime earthquake input energies. The earthquake input energies for controlled and uncontrolled systems are different as shown in the figure due to the response deduction in the controlled systems.

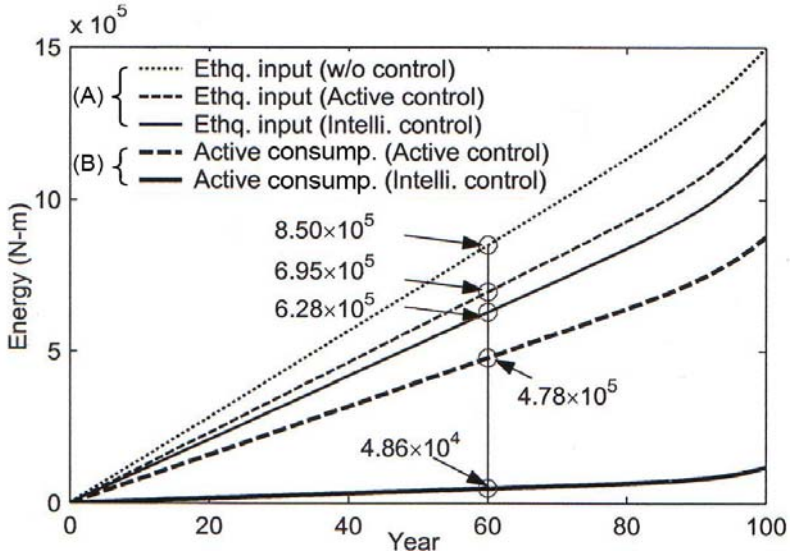

Figure 4 Accumulated input energies in building life time

To compare the energy difference from two control systems, the top floor displacement responses are set to the same for both the active and hybrid systems. Group B gives the accumulated active energies to be consumed relative to years of life for the time range of one hundred years. The values of energies in life span of sixty years are marked in Figure 4. It shows the much less active energy consumption in the hybrid control system with the intelligent algorithm in comparison to the active control system, 4.86×10^4 N-m versus 4.78×10^5 N-m. These results indicate that the building is less relied on the external active power while the proposed hybrid system is applied; therefore the hybrid system exhibits a better stability. The system maximally used the passive part in the intelligent strategy for most small and moderate earthquakes, in which the passive part is enough to restrict the response below the threshold and the active controller is not activated.

6. SUMMARY AND CONCLUSIONS

Considering the uncertainties of future earthquakes, a probability based analysis is proposed for structural control. A nondeterministic analysis is performed using the Monte Carlo method. Ground motions in each group of m_j=6.0, 7.0 and 8.0 are generated based on the seismic hazard at the building site. The results obtained from all ground motions in each group are statistically analyzed for maximum values of response, for which the extreme value distribution of Gumbel-type is applied.

Two types of control systems are studied: active control and hybrid control. For the hybrid control, an intelligent strategy is used to regulate the control process. PPF curves are proposed to be used in control performance evaluation in the expression of probability.

The required active controller capacity is evaluated based on the control force magnitude and the energy consumption per motion cycle. The hybrid control system requires much smaller capacity actuators than the

active control system to realize the same target of response reduction. The evaluation of the input energy in the building lifetime indicates that the intelligent algorithm in hybrid control systems can bring a more stable building system for relying less on the external power.

REFERENCES

Anagnos, T. and Kiremidjian, A.S. (1988). A review of earthquake occurrence models for seismic hazard analysis. *Probability Engineering Mechanics* **3:1**,3-11.

Beresnev, I.A., Atkinson G.M. (1999). Generic finite-fault model for ground-motion prediction in east-north America. *Bulletin of Seismological Society of America*, **3:** 608-625.

Boore D.M. (1983). Stochastic simulation of high-frequency ground motions based on seismological models of the radiated spectra. *Bulletin of Seismological Society of America*, **73:6**, 1865-1894.

Cheng, F.Y. (2001). Matrix Analysis Of Structural Dynamics: Application To Earthquake Engineering, Marcel Dekker, Inc., New York, NY, CRC Press/Taylor & Francis, Boca Raton, FL.

Cheng, F.Y., Tian, P., Rao, V., Martin, K., Liou, F., and Yeh, J.H. (1996). Theoretical and experimental studies on hybrid control of seismic structures. *Proceedings of the 12th ASCE Conference on Analysis and Computation*, Chicago, IL, 322-38.

Cheng, F.Y., Jiang, H.P. and Lou, K.Y. (2008). Smart Structures – Innovative Systems for Seismic Response Control, CRC Press/Taylor & Francis, Boca Raton, FL.

Darby R. (1976). Viscoelastic Fluids: An Introduction To Their Properties And Behavior, New York: M. Dekker.

Ellsworth, W.L., Matthews, M.V., Nadeau, R.M., Nishenko, S.P., Reasenberg, P.A., and Simpson, R.W. (1999). A physically-based earthquake recurrence model for estimation of long-term earthquake probabilities. *Workshop on Earthquake Recurrence: State of the Art and Directions for the Future*, Rome, Italy, 22-25.

Kotz, S., and Nadarajah, S. (2000). Extreme Value Distributions: Theory and Applications**,** Imperial College Press, River Edge, NJ.

Penzien, J., and Liu, S.C. (1969). Nondeterministic analysis of nonlinear structures to earthquake excitations. *Proceeding of 4th World Conference on Earthquake Engineering, Santiago*, Chile, Vol. I, sec. A-1.

Purcaru G. and Berckhemer H. (1978). A magnitude scale for very large earthquakes, *Techonophysics*, **49:** 189-198.

Sato R. (1979). Theoretical basis on relationships between focal parameters and earthquake magnitude, *Journal of Physics of the Earth*; **27:** 353-372.

Soong T.T., Dargush G.F. (1997). Passive Energy Dissipation Systems in Structural Engineering, New York: John Wiley & Sons Ltd.

Takahashi, Y.J., Kiureghian, A.D., and Ang, A.H-S. (2002). Decision methodology in Seismic Risk Management of a Single Building Based on Minimum Expected Life-Cycle Cost. Structural Engineering and Materials, University of California, Berkeley.

Zhang, X.Z., Cheng, F.Y. and Lou, M.L. (2004). Intelligent Hybrid Controlled Structures with Soil-structure Interaction. *Structural Engineering and Mechanics, An International Journal*, **17:3-4**, 573-591.

Zhang, X.Z., Cheng, F.Y., Lou M.L., Jiang, H.P. and Takahashi Y. (2004),Intelligent hybrid damper-actuator bracing control (HDABC) with deterministic and nondeterministic seismic input, soil-structure interaction, and tectonic movements, *Proceeding of 3rd International Conference on Earthquake Engineering, Nanjing, China.*

Zhang, X.Z., Cheng, F.Y. and Jiang, H.P. (2006), Hybrid actuator-damper-bracing control (HDABC) system with intelligent strategy and soil-structure interaction. *Engineering Structures, the Journal of Earthquake, Wind and Ocean Engineering,* **28**, 2010-2022.